

Critical Accretion Rate for Triggered Star Formation

Tomoyuki Hanawa¹ and Akihito Soeda¹

hanawa@cfs.chiba-u.ac.jp

ABSTRACT

We have reexamined the similarity solution for a self-gravitating isothermal gas sphere and examined implication to star formation in a turbulent cloud. When parameters are adequately chosen, the similarity solution expresses an accreting isothermal gas sphere bounded by a spherical shock wave. The mass and radius of the sphere increases in proportion to the time, while the central density decreases in proportion to the inverse square of time. The similarity solution is specified by the accretion rate and the infall velocity. The accretion rate has an upper limit for a given infall velocity. When the accretion rate is below the upper limit, there exist a pair of similarity solutions for a given set of the accretion rate and infall velocity. One of them is confirmed to be unstable against a spherical perturbation. This means that the gas sphere collapses to initiate star formation only when the accretion rate is larger than the upper limit. We have also examined stability of the similarity solution against non-spherical perturbation. Non-spherical perturbations are found to be damped.

Subject headings: accretion — hydrodynamics — shock waves — stars: formation

1. INTRODUCTION

Similarity solutions have contributed very much to our understanding of star formation process. The classical similarity solution by Larson (1969) and Penston (1969) elucidated the runaway nature of gravitational collapse. The density increases in proportion to the inverse square of the time during the runaway collapse phase. We learned from the similarity solutions of Shu (1977) and Hunter (1977) that the accretion rate of a protostar is of the order of c_s^3/G where G and c_s denote the gravitational constant and the isothermal sound speed of gas.

¹Center for Frontier Science, Chiba University, Inage-ku, Chiba, 263-8522, Japan

The similarity solution is also used to evaluate the effects of rotation and magnetic field. The similarity solutions of Narita, Hayashi, & Miyama (1984) and Saigo & Hanawa (1998) indicated that the runaway collapse cannot be prevented by rotation if once initiated. Collapse of a rotating magnetized gas cloud is described by the similarity solution of Krasnopolsky & Königl (2002). Ambipolar diffusion is taken into account in the the similarity solution of Adams & Shu (2007). Tsai & Hsu (1995) extended the similarity solution to include shock wave. Shu et al. (2002) extended the similarity solution involving a shock wave for application to champagne phase of an H II region.

Tsai & Hsu (1995) found two classes of similarity solution; the first class describes accretion onto protostar while the second one does failure of star formation. The central density decreases in proportion to the inverse square of the time, $\rho_c \propto t^{-2}$, in the second class solution. Although this solution has not gained much attention thus far, it provides an insight on dynamical compression of a molecular cloud core. If a dense clump of gas is compressed by an external force, the temporal increase in the density may trigger gravitational collapse and star formation. One can surmise existence of threshold of gravitational collapse. If the dynamical compression is either weak or short, the clump will bounce back to expansion. A shock wave will be formed when accreting gas is stopped by the expansion (Adams & Shu 2007, see, e.g.). The similarity solution of Tsai & Hsu (1995) demonstrated that a spherical cloud can expand even when it is steadily compressed by a shock wave. On the other hand, the shock compressed gas sphere will collapse owing to its self gravity if the shock is strong and lasts for a long enough period.

In this paper we reexamine the similarity solution of Tsai & Hsu (1995) while keeping its negative implication in mind. We find the condition for existence of similarity solution describing expansion of a gas sphere. Conversely it will tell us condition for a shock compressed gas sphere to collapse by its self gravity. We also study stability of the similarity solution. The similarity solution denies collapse due to the self gravity only when it is stable.

We review the similarity solution in §2.1 and show the method of linear stability analysis in §2.2. Technical details on the stability analysis are given in Appendix. Properties of similarity solutions, such as accretion rate and infall velocity, are shown in §3.1. Stability of the similarity solution is given in §3.2 and §3.3. We discuss implications of our analysis in §4.

2. Model and Methods of Computation

2.1. Similarity Solution

We consider an isothermal gas of which distribution is spherically symmetric. Then the hydrodynamical equations are expressed as

$$\frac{\partial \rho}{\partial t} + \frac{1}{r^2} \frac{\partial}{\partial r} (r^2 \rho v) = 0, \quad (1)$$

$$\frac{\partial v}{\partial t} + v \frac{\partial v}{\partial r} + \frac{1}{\rho} \frac{\partial P}{\partial r} + \frac{GM_r}{r^2} = 0, \quad (2)$$

and

$$\frac{\partial M_r}{\partial r} = 4\pi r^2 \rho \quad (3)$$

where

$$P = c_s^2 \rho. \quad (4)$$

Here, the symbols, ρ , v , P , M_r , G , and c_s denote the density, velocity, pressure, mass inside the radius r , gravitational constant, and the isothermal sound speed, respectively. As originally shown by Larson (1969) and Penston (1969), the hydrodynamical equations have similarity solutions,

$$\rho(r, t) = \frac{\varrho(\xi)}{4\pi G t^2}, \quad (5)$$

$$v(r, t) = \frac{u(\xi)}{c_s}, \quad (6)$$

$$M_r(r, t) = \frac{c_s^3 t}{G} \mu(\xi) \quad (7)$$

where

$$\xi = \frac{r}{c_s t}. \quad (8)$$

We restrict ourselves in the case of $t > 0$ in the following. Substituting Equations (5) through (8) into Equations (1) through (3) we obtain

$$\frac{\partial \varrho}{\partial \xi} = - \frac{[\mu - 2(\xi - u)^2] \varrho}{[(u - \xi)^2 - 1] \xi} \quad (9)$$

$$\frac{\partial u}{\partial \xi} = \frac{(\mu - 2)(\xi - u)}{[(u - \xi)^2 - 1] \xi} \quad (10)$$

and

$$\mu = \xi (\xi - u) \varrho. \quad (11)$$

We assume that the density is finite at the center since we are interested in application to a starless core, i.e., case of no star formation. Then the density and velocity should be expressed as

$$\varrho = \varrho_0 - \frac{\rho_0}{6} \left(\varrho_0 - \frac{2}{3} \right) \xi^2 + \frac{\rho_0}{45} \left(\varrho_0 - \frac{2}{3} \right) \left(\varrho_0 - \frac{1}{2} \right) + \mathcal{O}(\xi^6) \quad (12)$$

$$u = \frac{2\xi}{3} - \frac{\varrho_0}{45} \left(\varrho_0 - \frac{2}{3} \right) \xi^3 + \mathcal{O}(\xi^5) \quad (13)$$

near the center. Following Tsai & Hsu (1995) we assume that the flow has a shock wave at $\xi = \xi_{\text{sh}}$. Then the Rankine-Hugonio relation gives us the condition,

$$\frac{\varrho_+}{\varrho_-} = \frac{u_+ - \xi_{\text{sh}}}{u_- - \xi_{\text{sh}}}, \quad (14)$$

and

$$(u_+ - \xi_{\text{sh}})(u_- - \xi_{\text{sh}}) = 1. \quad (15)$$

where ϱ_+ and ϱ_- denote the the densities of the pre- and post-shocked gases, respectively, and u_+ and u_- do the velocities of them, respectively.

In the region far from the origin, a solution of Equations (9) and (10) approaches the asymptotic solution,

$$\varrho = \frac{\dot{M}}{v_{\text{inf}} \xi^2} + \mathcal{O}(\xi^{-3}), \quad (16)$$

$$u = -v_{\text{inf}} + \mathcal{O}(\xi^{-1}). \quad (17)$$

The symbol, v_{inf} , denotes the infall velocity at the infinity while \dot{M} denotes the accretion rate. The similarity solution can be specified either by $(\varrho_c, \xi_{\text{sh}})$ or by $(v_{\text{inf}}, \dot{M})$.

Note that Larson-Penston solution has the same asymptotic form. Only when v_{inf} and \dot{M} vanish, the solution Equations (9) and (10) have a different asymptotic form, “plus solutions” of Shu (1977).

We integrate equations (9) and (10) by the 4th order Runge-Kutta method from $\xi = 0$ for a given set of ϱ_c and ξ_{sh} to obtain a similarity solution. The infall velocity and accretion rate are obtained numerically as a function of ϱ_c and ξ_{sh} . We also obtain the mass enclosed in the shock front,

$$M_c = \int_0^{\xi_{\text{sh}}} \varrho \xi^2 d\xi. \quad (18)$$

2.2. Spherical and Non-spherical Perturbations

We have performed a normal mode analysis to examine the stability of the similarity solution. In the analysis, the density is assumed to be expressed as

$$\rho(r, t) = \frac{\varrho(\xi) + t^\sigma \delta\varrho(\xi) Y_\ell^m(\theta, \varphi)}{4\pi G t^2}, \quad (19)$$

where $Y_\ell^m(\theta, \varphi)$ denotes the spherical harmonic function. This particular form is chosen because the similarity solution has no specific timescale. An eigenmode has a growth timescale and an unstable perturbation grows exponentially, when the unperturbed state is stationary and has a specific timescale. When the physical quantities vary according to a power law in time in an unperturbed state, the eigenmode grows (or decay) in proportion to a power of time, $|t|^\sigma$. See Hanawa & Matsumoto (1999) for the justification of Equation (19). They analyzed linear stability of the Larson-Penston solution against a non-spherical perturbation, using the coordinates, $(\xi, \theta, \varphi, \ln t)$ instead of the ordinary spherical coordinates, (r, θ, φ, t) . It is shown that the similarity solution can be expressed as a steady state and an unstable mode grows in proportion to $\exp(\sigma \ln t) = t^\sigma$ in the coordinates.

The power index, σ , is obtained as an eigenvalue of the perturbation equations as shown in Appendix. When the real part of σ is positive, the mode grows in time and the similarity solution is unstable. We call the real part of σ , the growth index in the following according to the suggestion by F. H. Shu, the referee of this paper. When σ is complex, the mode grows (or decays) while oscillating. The imaginary part of σ is related with the frequency of oscillation, although the physical oscillation period increases with time.

3. Results

3.1. Similarity Solutions

First we obtained a series of similarity solutions for a given ϱ_c by increasing ξ_{sh} . The infall velocity, v_{inf} , decreases monotonically with increase in ξ_{sh} . It reaches $v_{\text{inf}} = 0$ at some ξ_{sh} and the similarity solution terminates. By compiling the similarity solutions, we obtained \dot{M} as a function of v_{inf} and ξ_{sh} . The curves denote \dot{M} as a function of ξ_{sh} for given v_{inf} in Figure 1.

The accretion rate, \dot{M} , is maximum at a certain ξ_{sh} for a given v_{inf} . It increases with increase in ξ_{sh} at a small ξ_{sh} while it decreases with increase in ξ_{sh} at a large ξ_{sh} . The former is denoted by thin curves while the latter is by thick ones. This means that there exists two similarity solutions for a given set of v_{inf} and \dot{M} .

Figure 2 shows two similarity solutions having $v_{\text{inf}} = 1.4$ and $\dot{M} = 1.204$. The solid curves denote the solution of $\xi_{\text{sh}} = 0.986$ while the dashed curves do that of $\xi_{\text{sh}} = 0.574$. Both the solutions have the same density and velocity distributions in the region of $\xi \geq 0.986$. The main difference is the location of the shock front. The shock compressed gas sphere is denser and expands more slowly in the solution denoted by the dashed curve. Since the expansion is slow, the solution is similar to the Bonnor (1956)-Ebert (1955) solution for a self-gravitating isothermal gas sphere. As well as the Bonnor-Ebert sphere, the latter solution is shown to be unstable (§3).

Figure 3 indicates that the similarity solution has an upper limit on \dot{M} for a given v_{inf} . The upper limit is highest $\dot{M}_{\text{max}} = 1.312$ at $v_{\text{inf}} = 1.64$. Similarity solutions do not exist for $\dot{M} > 1.312$. The implication of non-existence is discussed in §4.

3.2. Spherical Perturbations

Figure 4 shows the growth index of the spherical perturbation, σ_r , as a function of ξ_{sh} for a series of similarity solutions having a given v_{inf} . The solid curves denote the growth index of modes having real index. The dashed lines denote the real part of complex indices. One of the index is positive ($\sigma_r > 0$) and the similarity solution is unstable only when the shock radius (ξ_{sh}) is smaller than a critical value. The condition of neutral stability coincides with that of maximum accretion rate for a given v_{inf} as expected. When ξ_{sh} is a little larger than the critical, the solution is stable and the most slowly damping mode has a real index. When ξ_{sh} is large enough, the solution is stable and the most slowly damping mode has a complex index.

Our survey is limited to modes having low indices, i.e., in the range $|\sigma_i| \leq 1.0$. It is however unlikely that we have missed unstable spherical perturbations. A spherical perturbation induces only sound waves and they are confined within the gas sphere since it is bounded by the shock wave. A high frequency sound wave has a shorter wavelength and is unlikely to be Jeans unstable.

3.3. $\ell = 2$ Mode

We have studied $\ell = 2$ mode as a typical non-spherical perturbation. This is in part because the dipole ($\ell = 1$) mode is unlikely to be excited. If the dipole mode grows, the inner and outer parts of the gas sphere should move in the opposite direction each other to keep the center of gravity.

Figure 6 denotes the eigenfrequencies of the $\ell = 2$ modes for similarity solutions of $v_{\text{inf}} = 1.0$. The abscissa denotes ξ_{sh} while the ordinate denotes the index, σ . All the modes are damping ($\sigma_i < -1$). The solid lines denote the mode having the smallest damping index. The mode has a small imaginary part ($\sigma_i \simeq \pm 0.1$). The mode having the second smallest damping index is denoted by the dashed line in Figure 6 and has a real eigenfrequency (pure damping). The mode having the third smallest damping index has an imaginary part in the eigenfrequency. The imaginary part is similar to that of the mode having the smallest damping index. These three modes have a similar damping index of $-1.1 \leq \sigma_r \leq -1.0$. The other mode (dash-dotted line in Fig. 6) has a much larger damping index.

Figure 7 is the same as Figure 6 but for $v_{\text{inf}} = 4.0$. Again, all the modes are damping. The damping index is larger than unity ($\sigma_r < -1$). The oscillation frequency of the smallest damping mode is larger than those of $v_{\text{inf}} = 1.0$.

One might ask the reason why the similarity solution is stable against a bar ($\ell = 2$) mode. We think that the bar mode is damped by expansion of the gas sphere. Since the radius of the shock front increases with the time, the asphericity of the shock compressed gas sphere decreases unless the displacement grows faster than the radius. When a gas sphere is collapse, the bar mode can be excited as shown by Lin, Mestel, & Shu (1965) for the pressure less gas and Hanawa & Matsumoto (1999) for an isothermal gas.

We have not yet studied the modes of $\ell \geq 3$. However they are also unlikely to be unstable, since the self-gravity does not excite a short wave perturbation.

4. Discussion

We obtained the critical accretion rate above which there exists no similarity solution. The critical rate can be interpreted as the minimum accretion rate for a high density clump to initiate self-gravitational collapse. The critical accretion rate can be rewritten as

$$\left. \frac{dM}{dt} \right|_{\text{cr}} = \frac{3.6 c_s^4}{Gv}, \quad (20)$$

for $v \gtrsim 3c_s$ in the dimensional form.

Equation (20) gives us an estimate for a converging flow to initiate gravitational collapse. We shall consider a spherical region of which surface is surrounded by a converging flow. The radius, inflow velocity, and density are assumed to be r , v and ρ , respectively. Then the gravitational collapse will be initiated when the mass accretion rate exceeds the critical,

$$4\pi r^2 \rho v > \frac{3.6 c_s^4}{Gv}. \quad (21)$$

Equation (21) can be rewritten as

$$\frac{2r}{\lambda_J} > \frac{0.3 c_s}{v}, \quad (22)$$

where

$$\lambda_J = \frac{2\pi c_s}{\sqrt{4\pi G\rho}}. \quad (23)$$

Since λ_J denotes the Jeans length, Equation (22) means that the effective Jeans length reduces in proportion to the inverse of the Mach number.

The Jeans mass is proportional to the cube of the Jeans length for a given density. Thus the effective Jeans mass should reduce to

$$M_{J, \text{eff}} = M_J \left(\frac{\lambda_{J, \text{eff}}}{\lambda_J} \right)^3 \quad (24)$$

$$= M_J \left(\frac{v}{0.3 c_s} \right)^{-3}. \quad (25)$$

This implies that compression of sub Jeans mass clump may result in gravitational collapse in the region of flow convergence. Note that the effective Jeans mass is several order of magnitude smaller than the classical one when $v \gtrsim 3 c_s$.

The compression should continue for a certain timescale for a dynamically compressed clump to collapse by its self gravity. If we evaluate the minimum timescale to be the effective Jeans length divided by the flow velocity, it is shorter than the free-fall timescale by a factor of the Mach number squared,

$$\tau_{\text{comp}} \simeq \frac{\lambda_{J, \text{eff}}}{v} \simeq \tau_{\text{ff}} \left(\frac{v}{c_s} \right)^{-2}. \quad (26)$$

The timescale can be translated into the wavelength of perturbation. A compressed clump can collapse by the self gravity if the wavelength of velocity perturbation is longer than the effective Jeans length. If turbulence contains velocity perturbations of long wavelengths, gravitational collapse due to dynamical compression will take place somewhere in the cloud. In such case we can expect a number of clumps of which masses are much smaller than the classical Jeans mass.

We thank T. Matsumoto and F. Nakamura for discussion and valuable comments on the original manuscript. We also thank F. H. Shu for his valuable comments as the referee. We have added comparison of Tsai & Hsu (1995) solution with Bonnor-Ebert solution in the revised manuscript according to the comments given to the original manuscript. This

study is financially supported in part by the Grant-in-Aid for Scientific Research on Priority Area (19015003) of The Ministry of Education, Culture, Sports, Science, and Technology (MEXT).

A. Linear Stability Analysis

Since the density is given by Equation (19) in our linear stability analysis, the gravitational potential should be expressed as

$$\Phi(r, t) = c_s^2 [\psi(\xi) + t^\sigma \delta\psi(\xi) Y_\ell^m(\theta, \varphi)]. \quad (\text{A1})$$

The velocity, $\mathbf{v} = (v_r, v_\theta, v_\varphi)$, is assumed to be expressed as

$$v_r(r, t) = c_s [u(\xi) + t^\sigma \delta u_r Y_\ell^m(\theta, \varphi)], \quad (\text{A2})$$

$$v_\theta(r, t) = -c_s t^\sigma \frac{\delta u_\theta(\xi)}{\ell + 1} \frac{\partial}{\partial \theta} Y_\ell^m(\theta, \varphi), \quad (\text{A3})$$

$$v_\varphi(r, t) = -c_s t^\sigma \frac{\delta u_\theta(\xi)}{(\ell + 1) \sin \theta} \frac{\partial}{\partial \varphi} Y_\ell^m(\theta, \varphi), \quad (\text{A4})$$

in the spherical coordinates. We assume that the perturbation is vanishingly small in the region very far from the center. In other words, we restrict ourselves to search for an instability due to the internal structure of the shock compressed gas sphere. Thus the flow is assumed to have no vorticity,

$$(\ell + 1) \delta u_r + \frac{d}{d\xi} (\xi \delta u_\theta) = 0. \quad (\text{A5})$$

The assumption of no vorticity is based on the Kelvin's circulation theorem. It says the circulation,

$$\Gamma \equiv \oint_C \mathbf{u} \cdot d\mathbf{u} \quad (\text{A6})$$

is conserved for an isothermal (barotropic) gas (see, e.g., Chapter 6 of Shu 1992). Since the Lagrangian loop C expands, the circulation velocity should decrease with the time to conserve Γ , although it can grow with the time if measured at a given ξ . See Hanawa & Matsumoto (2000) for more details on the mathematical treatment of perturbations having vorticity.

After some manipulation, the perturbation equations are written as

$$(\sigma + 1) \delta \varrho + \frac{1}{\xi^2} \frac{d}{d\xi} (\xi^2 \delta f) + \frac{\ell \varrho_0 \delta u_\theta}{\xi} = 0, \quad (\text{A7})$$

$$\begin{aligned}
 (\sigma + 2) \delta f + \frac{1}{\xi^2} \{ \xi^2 [2w \delta f + (1 - w^2)] \} \\
 - \left(\varrho_0 w + \frac{2}{\xi} \right) \delta \varrho + \varrho_0 \delta \gamma + \frac{\ell \varrho_0 w \delta u_\theta}{\xi} = 0, \tag{A8}
 \end{aligned}$$

$$\frac{d}{d\xi} \delta \psi = \delta \gamma, \tag{A9}$$

$$\frac{d}{d\xi} \delta \gamma = \delta \varrho - \frac{2 \delta \gamma}{\xi} - \frac{\ell (\ell + 1)}{\xi^2} \delta \psi \tag{A10}$$

where

$$w = u - \xi, \tag{A11}$$

$$\delta u_\theta = \frac{\ell + 1}{(\sigma + 1) \xi} \left(w \delta u_r + \frac{\delta \varrho}{\varrho_0} + \delta \psi \right), \tag{A12}$$

$$\delta f = \varrho_0 \delta u_r + w \delta \varrho, \tag{A13}$$

$$\delta \gamma = \frac{\partial}{\partial \xi} \delta \psi. \tag{A14}$$

The perturbation equations do not contain the azimuthal wavenumber, m , and accordingly thus the growth rate does not depend on m . This is because the unperturbed state (similarity solution) is spherically symmetric.

We must consider the jump condition at the shock front as well as the boundary conditions to solve the perturbation equation. The density perturbation is discontinuous between the pre- and post-shocked flows and contains change due to shift of the shock front. The latter introduces the Dirac's delta function proportional to the shift and the density difference between the pre- and post flows. After some manipulation we obtain the jump condition,

$$(w_+ - w_-) [\delta f] - (\varrho_+ - \varrho_-) \left[w \delta u_r + \frac{\delta \varrho}{\varrho_0} \right] = 0, \tag{A15}$$

$$(\sigma + 1) [\delta \gamma] + [\delta f] = 0 \tag{A16}$$

where the bracket denotes the difference between $\xi = \xi_{\text{sh}} \pm \varepsilon$. The symbols with the subscripts, + and –, denote the values at $\xi = \xi_{\text{sh}} \pm \varepsilon$, respectively. The perturbation in the potential, $\delta \psi$, is continuous even at $\xi = \xi_{\text{sh}}$. These jump conditions enable us to connect the perturbation in the post-shocked flow ($\xi < \xi_{\text{sh}}$) and that in the pre-shocked flow ($\xi > \xi_{\text{sh}}$).

When the perturbation is spherically symmetric ($\ell = 0$), Equations (A7) and (A10) are linearly dependent and we obtain

$$\delta \gamma = - \frac{\delta f}{\sigma + 1} \tag{A17}$$

for $\ell = 0$. Thus we need two independent boundary conditions for $\ell = 0$ and three for $\ell \neq 0$.

The spherical perturbation should vanish in the pre-shocked since the unperturbed flow is supersonic. Otherwise the perturbation diverges when the mode is unstable. Thus the effective outer boundary is set at $\xi = \xi_{\text{sh}}$ and the jump condition is applied there. The other boundary condition is set so that the velocity perturbation vanishes at the origin, $\xi = 0$ and is proportional to ξ near the origin. We have integrated the perturbation equation numerically with the Runge-Kutta method from the origin and searched the eigenvalue, σ , by try and error.

Non-spherical perturbations should also be regular at the origin and vanishingly small at infinity. We calculated asymptotic solutions around the origin and those around the infinity to examine the condition for perturbations to be regular according to Hanawa & Matsumoto (1999). Some asymptotic solutions are divergent since the perturbation equations are singular at the origin and infinity. When $\ell \neq 0$, the perturbation should be expressed by the asymptotic solution,

$$\delta \varrho = B \varrho_0 \xi^\ell, \quad (\text{A18})$$

$$\delta u_r = -A \ell \xi^{\ell-1} - C(\ell + 2) \xi^{\ell+1}, \quad (\text{A19})$$

$$\delta \psi = \left[A \left(\sigma + 1 - \frac{\ell}{3} \right) - B \right] \xi^\ell, \quad (\text{A20})$$

where

$$C = \frac{1}{4\ell + 6} \left[\frac{\ell}{3} \left(\varrho_0 - \frac{2}{3} \right) A + \left(\sigma - \frac{\ell - 1}{3} \right) B \right]. \quad (\text{A21})$$

Here the symbols, A and B , denote arbitrary constants. Equations (A18) and (A20) mean that the density and potential perturbations can be expanded by a series of polynomials starting from the ℓ -th power in the Cartesian coordinates. Otherwise the perturbation diverges at the origin. The velocity perturbation is also expanded by another series of polynomials starting from the $(\ell - 1)$ -th order since it should be balanced with gradient of the potential perturbation.

The other boundary condition is given by the asymptotic solution,

$$\delta \varrho = \frac{2D(\ell + 1) \varrho_0}{(\sigma + \ell + 2)(\sigma + \ell + 3) \xi^{\ell+3}}, \quad (\text{A22})$$

$$\delta u_r = \frac{D(\ell + 1)}{(\sigma + \ell + 2) \xi^{\ell+2}}, \quad (\text{A23})$$

$$\delta \psi = \frac{D}{\xi^{\ell+1}}, \quad (\text{A24})$$

for $\xi \gg 1$. Here, the symbol D denotes an arbitrary constant. Equation (A24) means that the potential perturbation in the region $\xi \gg 1$ is dominated by the aspherical density distribution near the center. In other words the density perturbation is too small to affect the gravitational potential. Equation (A23) means that the velocity perturbation is induced by the gravitational perturbation. Equation (A22) means that the density perturbation is induced by the velocity perturbation. Thus our boundary conditions guarantee that the perturbation is induced by internal change in the flow.

We integrated the perturbation equations both from the origin ($\xi = 10^{-2}$) and a very large ξ ($\simeq 100$) with the Runge-Kutta method. We surveyed the eigenvalue, σ , by examining whether the numerical solutions from both ends satisfy the jump condition at the shock front.

REFERENCES

- Adams, F. C., & Shu, F. H. 2007, *ApJ*, 671, 497
- Bonnor, W. B. 1956, *MNRAS*, 116, 351
- Ebert, R. 1955, *ZAp*, 37, 217
- Hanawa, T., & Matsumoto, T. 1999, *ApJ*, 521, 703
- Hanawa, T., & Matsumoto, T. 2000, *ApJ*, 540, 962
- Hunter, C. 1977, *ApJ*, 218, 834
- Krasnopolsky, R., & Königl, A. 2002, *ApJ*, 580, 987
- Larson, R. B. 1969, *MNRAS*, 145, 271
- Larson, R. B. 2003, *Reports on Progress in Physics*, 66, 1651
- Lin, C. C., Mestel, L., & Shu, F. H. 1965, *ApJ*, 143, 1431
- Narita, S., Hayashi, C., Miyama, S. M. 1984, *Prog. Theor. Phys.*, 72, 1118
- Penston, M. V. 1969, *MNRAS*, 144, 425
- Saigo, K., & Hanawa, T. 1998, *ApJ*, 493, 342
- Shu, F. H. 1977, *ApJ*, 214, 488

Shu, F. H. 1992, *The Physics of Astrophysics Volume II Gas Dynamics*, (Mill Valley, University Science Books)

Shu, F. H., Lizano, S., Galli, D., Cantó, J. & Laughlin, G. 2002, *ApJ*, 580, 969

Tsai, J. C., Hsu, J. J. L. *ApJ*, 448, 774

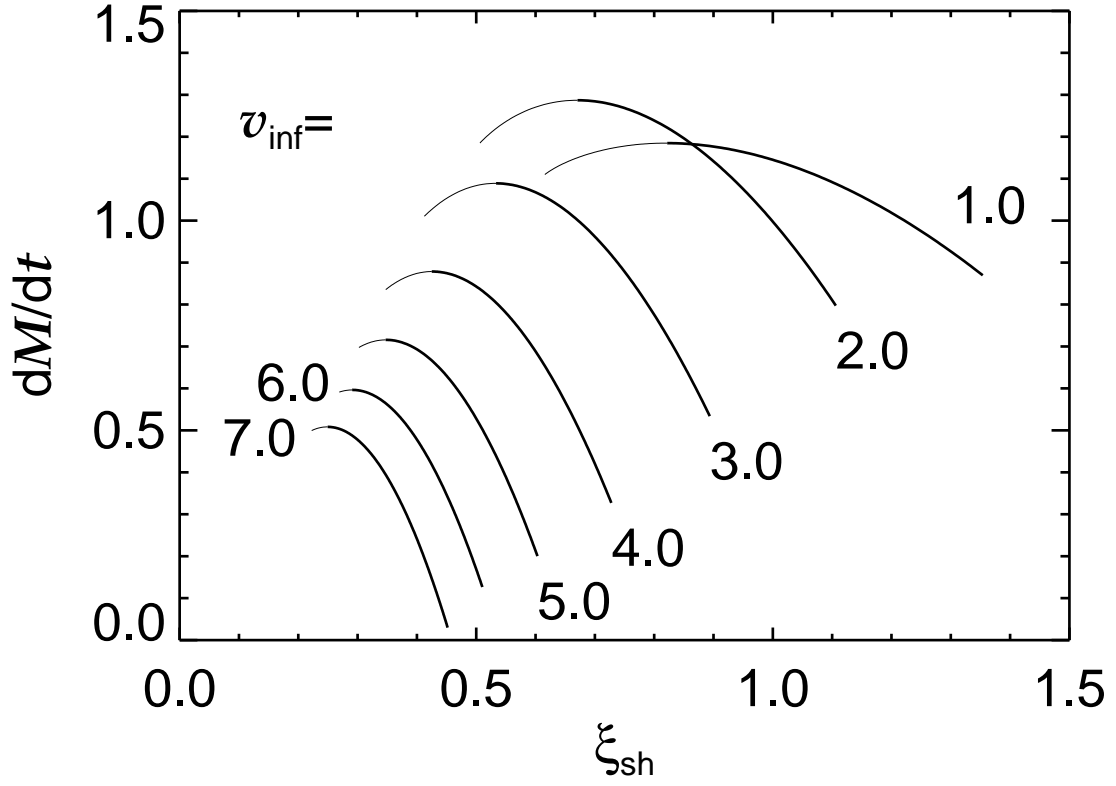


Fig. 1.— The accretion rate, \dot{M} , is shown as a function of ξ_{sh} for a given v_{inf} .

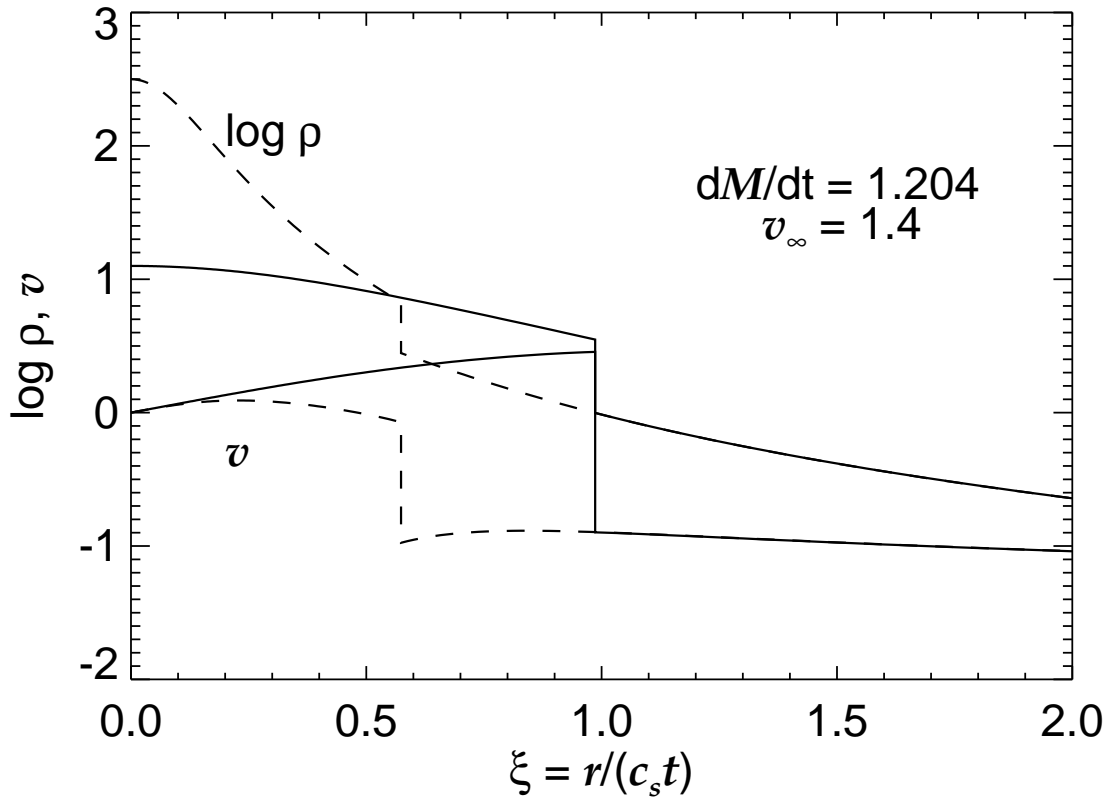


Fig. 2.— The density and velocity distributions are shown for two similarity solutions having the same v_{inf} and dM/dt .

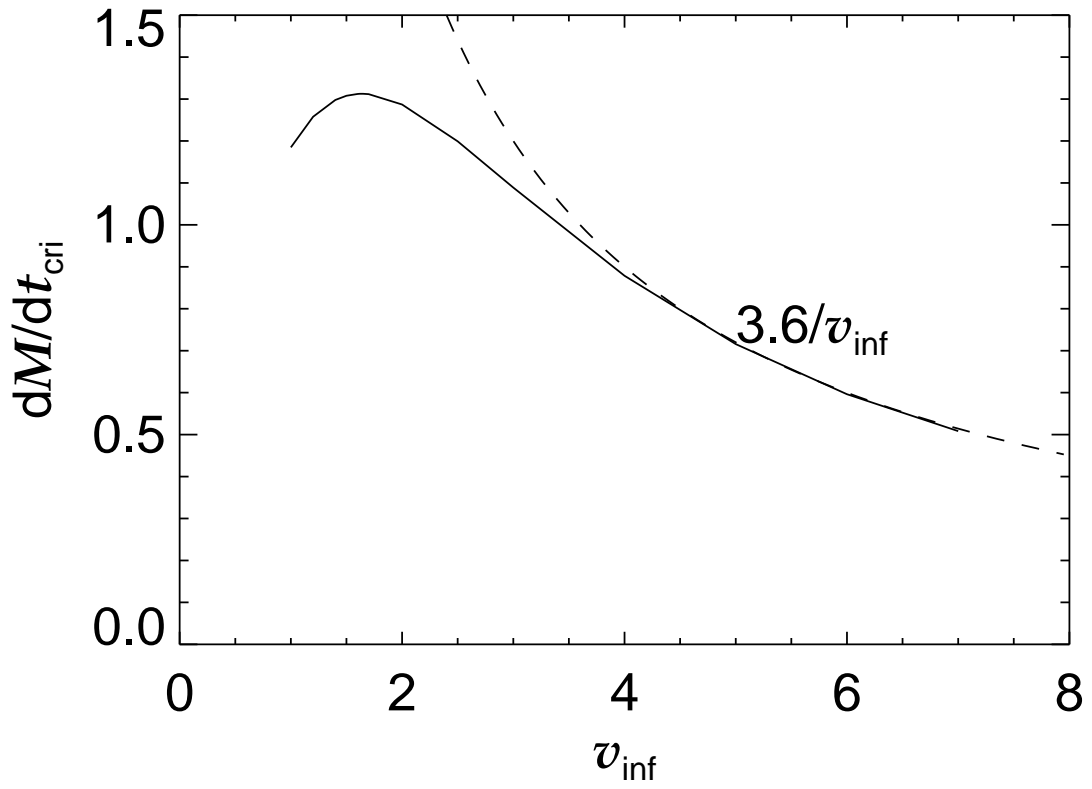


Fig. 3.— The critical accretion rate is shown as a function of v_{inf} .

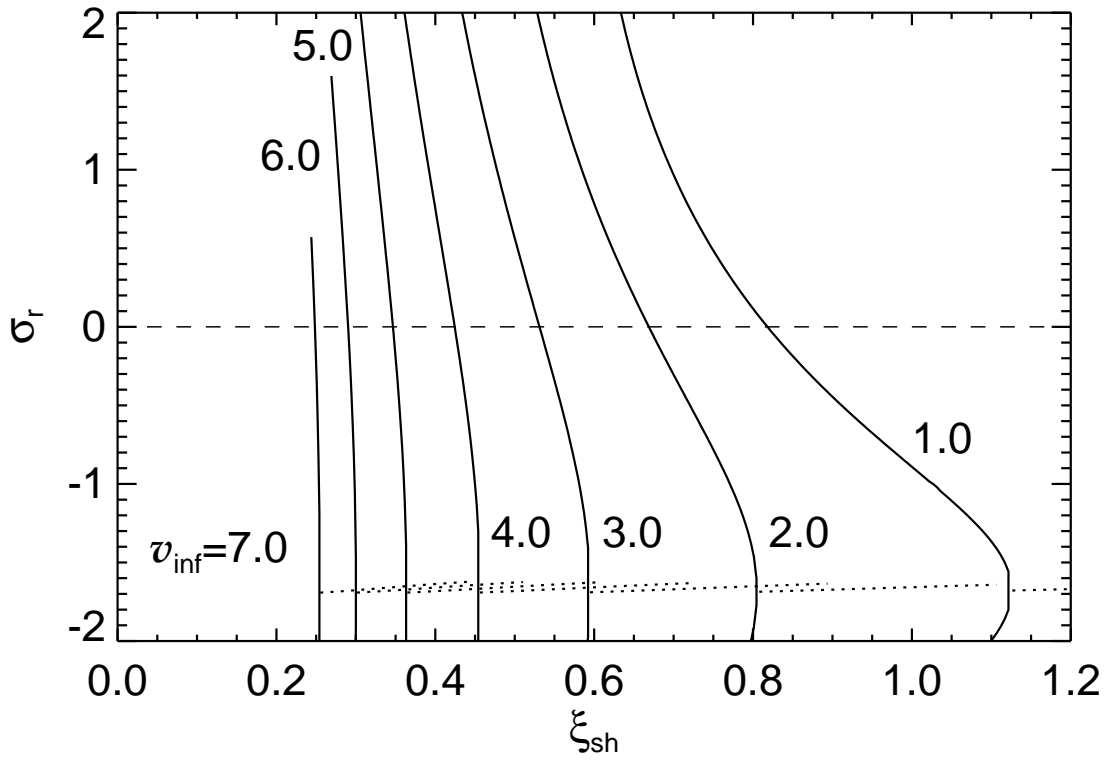


Fig. 4.— Each curve denotes the real part of eigenfrequency, σ_r , of a spherical perturbation as a function of the shock radius, ξ_{sh} for a given v_{inf} .

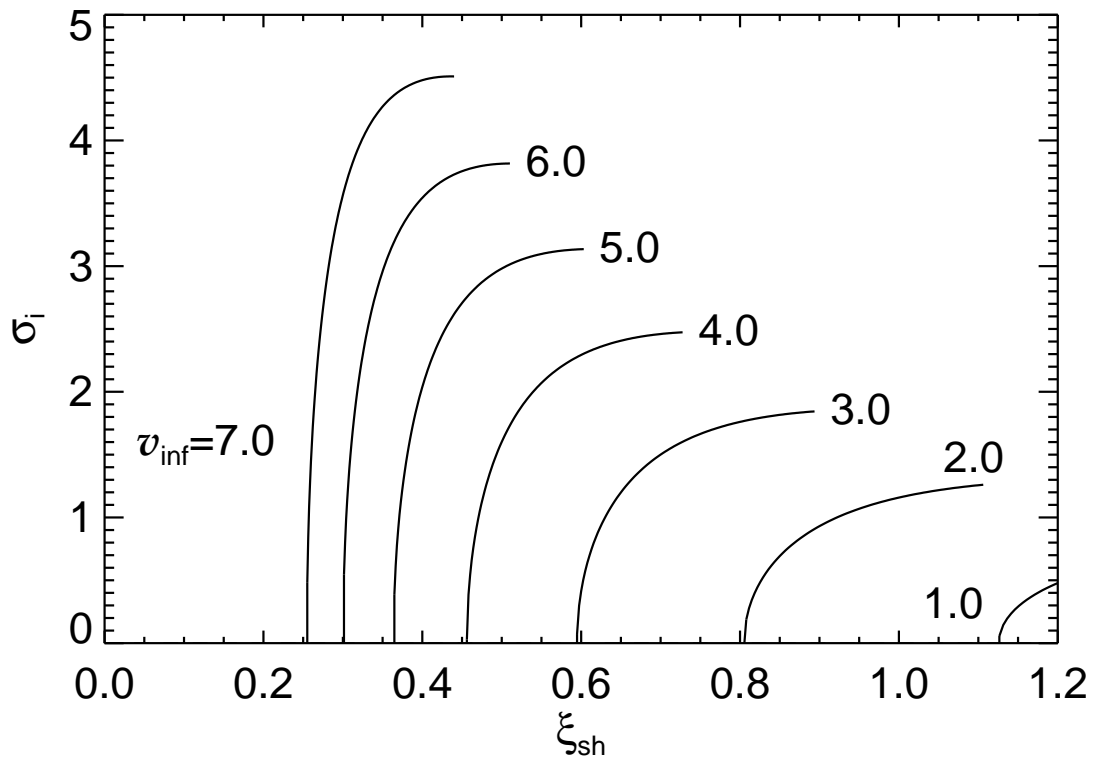


Fig. 5.— The same as Fig. 4 but for the imaginary part, σ_i .

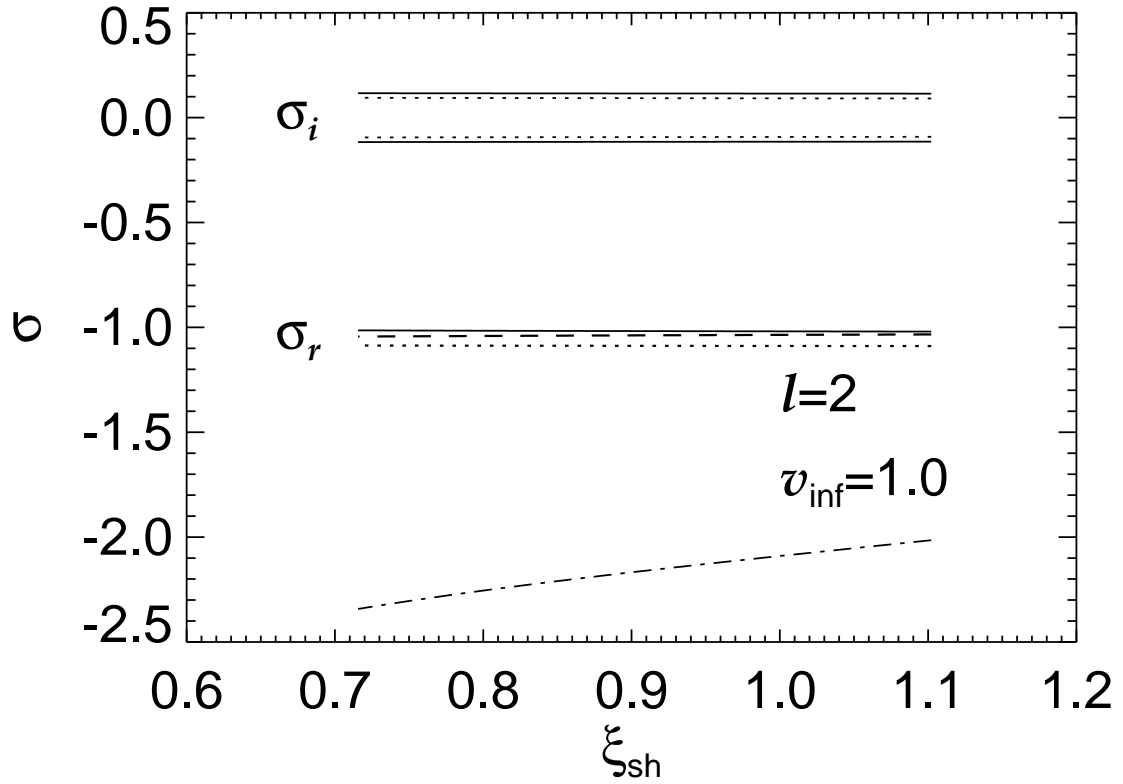


Fig. 6.— The eigenfrequency, σ , is shown as a function of ξ_{sh} for similarity solutions having $v_{\text{inf}} = 1.0$. The solid curves denote the real part of σ for non-spherical perturbations having $\ell = 2$, while dashed curves do that of imaginary part. Mode a has complex eigenfrequencies while modes b and c have real eigenfrequencies.

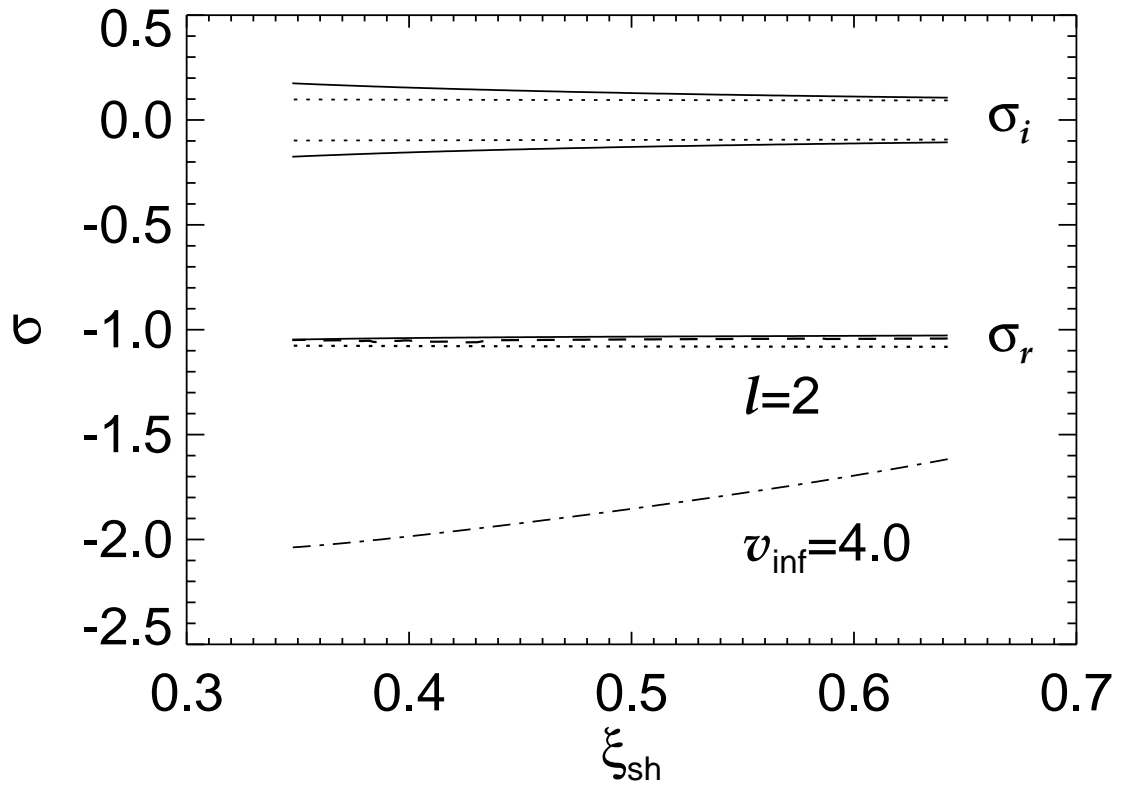


Fig. 7.— The same as Fig. 6 but for $v_{\text{inf}} = 4$.